

# AB Dor Moving Group Stars Resolved with the CHARA Array

G. H. Schaefer<sup>1</sup>, R. J. White<sup>2</sup>, E. K. Baines<sup>3</sup>, T. S. Boyajian<sup>4</sup>, T. A. ten Brummelaar<sup>1</sup>, C. D. Farrington<sup>1</sup>, J. Sturmann<sup>1</sup>, L. Sturmann<sup>1</sup>, and N. H. Turner<sup>1</sup>

<sup>1</sup> The CHARA Array of Georgia State University, Mount Wilson Observatory, Mount Wilson, CA 91023, USA; schaefer@chara-array.org.
 <sup>2</sup> Center for High Angular Resolution Astronomy and Department of Physics and Astronomy, Georgia State University, P.O. Box 4106, Atlanta, GA 30302, USA
 <sup>3</sup> Remote Sensing Division, Naval Research Laboratory, 4555 Overlook Avenue SW, Washington, DC 20375, USA
 <sup>4</sup> Department of Physics & Astronomy, Louisiana State University, Baton Rouge, LA 70803, USA
 Received 2017 July 13; revised 2018 February 5; accepted 2018 March 23; published 2018 May 7

#### **Abstract**

We present interferometric measurements obtained with the CHARA Array of 13 adolescent-age stars in nearby moving groups. The motivation was to spatially resolve the largest stars and to search for binary companions. Nine stars have diameters smaller than the resolution limit and no evidence for companions within 0.5–50 mas and  $\Delta H < 2.0$  mag. The diameters of three stars were spatially resolved: GJ 159 (0.582  $\pm$  0.016 mas) and GJ 393 (0.564  $\pm$  0.021 mas) in the AB Dor moving group, and former member HD 89744 (0.556  $\pm$  0.032 mas). Combining the angular diameters with their distances and bolometric fluxes, we measured radii and effective temperatures. The temperatures of GJ 159 (6286  $\pm$  123 K) and GJ 393 (3515  $\pm$  68 K) are consistent with spectroscopic measurements. Comparisons with evolutionary models show that HD 89744 has evolved off the main sequence. GJ 159 and GJ 393 lie within 1.5 $\sigma$  of the zero-age main sequence, complicating their age estimates because it is unclear whether the stars are contracting or expanding. GJ 159 has a mass of 1.2  $\pm$  0.1  $M_{\odot}$  with an age spanning 0.021–3.0 Gyr. Its debris disk and lithium abundance favor a young age. GJ 393 has a mass of 0.42  $\pm$  0.03  $M_{\odot}$  and a lower limit on its age 0.06 Gyr. This overlaps with the age of the moving group; however, an older age would be more consistent with its slow rotation, low activity, and luminosity, suggesting that GJ 393 is a kinematic interloper.

Key words: stars: fundamental parameters – stars: individual (GJ 159, GJ 393, HD 89744) – stars: pre-main sequence – techniques: interferometric

Supporting material: machine-readable table

#### 1. Introduction

The prospects for conducting detailed studies of young stars and young planetary systems improved greatly with the discovery of associations of stars with ages of 10–100 Myr in close proximity (<100 pc) to the Sun (e.g., Zuckerman & Song 2004; Torres et al. 2008). For example, studies of stars in these associations have led to high-fidelity images of disks (e.g., AU Mic, TW Hya; Kalas et al. 2004; Liu 2004; Nomura et al. 2016) and directly imaged planet-mass objects (e.g., 2M1207b, WISEA J114724.10-204021.3; Chauvin et al. 2004; Schneider et al. 2016). New instruments and facilities have been commissioned and are being constructed with the primary science goal of looking for planets and disks around these nearby young stars (e.g., Kataria & Simon 2010).

The temporal evolution of young stars, brown dwarfs, debris disks, and extrasolar planets in these associations is limited by our understanding of their ages. Although it is believed that these associations consist of coeval populations, their adolescent age makes assigning absolute ages difficult. This is in part because at ages older than  $\sim 30$  Myr, solar-mass stars have already gravitationally settled to their main sequence size, thus they are not distinctively overluminous. While lower-mass (e.g.,  $<0.5~M_{\odot}$ ) members are predicted to still be gravitationally contracting, the use of these stars for constraining ages has been inhibited by both poorly determined stellar properties (effective temperatures, bolometric luminosities, and multiplicity) and limitations of the stellar evolutionary models. As an example, while most low-mass association members have a measured spectral type, it is uncertain whether to assign a dwarf-like temperature to these stars or a slightly warmer temperature as is

adopted for T Tauri age stars (e.g., White et al. 1999; Luhman et al. 2003; Pecaut & Mamajek 2013). Moreover, most theoretical isochrones do a poor job of matching the main sequence below  $0.5~M_{\odot}$  as defined empirically by either nearby field stars (e.g., Hillenbrand & White 2004) or open clusters (e.g., Stauffer et al. 2007; Bell et al. 2012); discrepancies are attributed to uncertainties in the requisite input physics.

The high spatial resolution achieved by long-baseline optical/infrared interferometry provides a powerful tool for overcoming these limitations. First, interferometric measurements can be used to spatially resolve short-period spectroscopic binaries to determine accurate dynamical masses. These in turn can be used to constrain the input physics of stellar evolutionary models (e.g., Boden et al. 2007; Le Bouquin et al. 2014). Second, the close proximity of these young stellar populations imply that at least some of the stars can be spatially resolved (McCarthy & White 2012), yielding direct measures of stellar radii. If stellar luminosities are determined from spectral energy distributions (SEDs), these radii can be used to determine accurate stellar effective temperatures through Stefan's Law; temperatures with precision of  $\sim$ 1%–2% are now regularly achieved from interferometric data (Boyajian et al. 2012b, 2013). Simon & Schaefer (2011) demonstrated the success of measuring interferometric sizes of two F star members of the  $\beta$  Pictoris moving group. The radius measurements indicate an age of  $13 \pm 2$  Myr, which is toward the lower end of the 10-24 Myr range of age determinations (see Mamajek & Bell 2014 and references therein).

With these goals in mind, we present an interferometric survey of 13 young candidate members of nearby moving groups, the majority (nine) of which are in the AB Doradus

**Table 1**Observed Sample of Stars<sup>a</sup>

Name	HD	HIP	Group <sup>b</sup>	SpT <sup>c</sup>	Dist <sup>d</sup> (pc)	$V^{\mathrm{c}}$	K <sup>c</sup>
PW And	1405		AB Dor	K2	27	8.859	6.39
BD+23 296 A	13482	10272	AB Dor	K1*	$36.6 \pm 1.6$	7.932	5.73*
BD+28 382	14082A	10680	$\beta$ Pic	F8	$34.5 \pm 3.4$	7.031	5.79
BD+28 382B	14082B	10679	$\beta$ Pic	G1	$27.3 \pm 4.4$	7.755	6.26
BD-04 560	20385	15247	Tuc/Hor	F5	$49.2 \pm 1.4$		6.10
V577 Per A	21845	16563	AB Dor	G5	$34.4 \pm 1.2$	8.250	6.37
GJ 159	25457	18859	AB Dor	F8	$18.83 \pm 0.11$	5.378	4.18
BD+20 1790			AB Dor	K5	26	10.215	6.88
BD+41 2076	89744	50786	[AB Dor]	F7	$39.43 \pm 0.48$	5.720	4.45
GJ 393		51317	[AB Dor]	M2.5	$7.07 \pm 0.11$	9.586	5.31
PX Vir AB	113449	63742	AB Dor	K1*	$21.69 \pm 0.38$	$7.700^{*}$	5.51*
BD-04 4194	152555	82688	AB Dor	G0	$46.7 \pm 2.0$	7.818	6.36
LO Peg, GJ 4199		106231	AB Dor	K5	$24.8 \pm 0.65$	9.245	6.38

#### Notes.

moving group. Age estimates for this group range from 50 to 150 Myr (e.g., Malo et al. 2013; Bell et al. 2015). The primary motivation of the survey was to spatially resolve stars that are large enough to be resolved to measure their radii and effective temperatures, and to search for binary companions at milliarcsecond (mas) separations.

# 2. Sample Selection, Observations, and Data Reduction

### 2.1. Moving Group Members

At the inception of this project in 2008, stars were selected for interferometric observations from the moving group membership lists assembled in Zuckerman & Song (2004) and López-Santiago et al. (2006). Since then, the membership lists have been expanded through further kinematic studies (e.g., Schlieder et al. 2010; Aller et al. 2016; Riedel et al. 2017). Based on the typical sensitivities<sup>5</sup> of the CHARA Array at the time when we began the survey, we restricted the sample to stars brighter than K < 6.5 mag and V < 10 mag. We also required the stars to be located northward of decl.  $> -5^{\circ}$ . Although stars can be observed at lower elevations in the sky, we used a conservative limit so that the targets could be observed at low airmasses for several hours during the night to ensure good visibility calibration.

From the initial sample, we removed four stars (GJ 856, HD 4277, HD 17332, and HIP 23418) that had known binary companions with separations between 1" and 4" (e.g., Mason et al. 2001). Given the diffraction-limited resolution of an individual CHARA telescope (1"6 in the *K*-band for a 1 m diameter mirror) and typical seeing conditions, incoherent light from the companion would degrade the fringe visibility of the primary star. Before we realized the nature of these complications, we observed HD 13482 which has a 1"8 companion (Mason et al. 2007).

HD 29391 fell within the selection criteria of our survey, but it had been resolved previously by Simon & Schaefer (2011) using the CHARA Array. We also did not observe HD 129333,

because at a decl. of  $+64^{\circ}$ , it was in a different part of the sky compared with other targets in the sample and could not be observed with the same configuration of the array. We added one fainter star to our sample, BD+20 1790, to fill an empty window in our scheduled time.

The total sample observed consists of 13 stars: 10 proposed AB Dor members, two  $\beta$  Pic members, and one Tucana/Horologium member. However, since the sample was originally defined, several more rigorous membership studies have been conducted and neither Malo et al. (2013) nor Bell et al. (2015) consider HD 89744 to be a member of the AB Dor moving group. Further evidence against its membership based on its evolved age is presented in Section 5. GJ 393 is considered a bona fide member of the AB Dor moving group by Malo et al. (2013); however, Bell et al. (2015) determine it to be  $\sim$ 0.5 mag below an empirical single-star isochrone for the AB Dor moving group. They do not consider it to be a member, despite its consistent kinematic properties. The remaining 11 stars are considered bona fide members in both studies.

All 13 stars are listed in Table 1 by their common name, Henry Draper number, and *Hipparcos* number (when available); the name used in this document is highlighted in boldface type in Table 1 for clarity. The spectral types are from either the spectroscopic study of McCarthy & White (2012) or the original membership survey (Zuckerman & Song 2004; López-Santiago et al. 2006). The *V*-band magnitudes are calculated from  $V_T$  magnitudes in the Tycho-2 Catalog (Høg et al. 2000), using the prescription of Bessell (2000). The  $K_s$  magnitudes are from 2MASS (Skrutskie et al. 2006).

Six of the observed stars are members of multiple star systems. As mentioned before, HD 13482 has a 1.18 companion (Mason et al. 2007). PX Vir has a companion detected spectroscopically with a period of 216 days (Griffin 2010; Guenther & Tal-Or 2010) and resolved spatially with a semimajor axis of  $\sim 0.1910$  and flux ratio of  $\Delta H = 1.6$  mag (Evans et al. 2012). Although the primary stars in the HD 13482 and PX Vir systems dominate the emitted optical/infrared light, the majority of observed properties listed in Table 1 are from spatially unresolved measurements, and therefore are likely biased. The two  $\beta$  Pic members observed

<sup>&</sup>lt;sup>a</sup> The star name used in this document is highlighted in boldface type.

<sup>&</sup>lt;sup>b</sup> The moving group identification is listed in square brackets if the star is no longer considered to be a member.

<sup>&</sup>lt;sup>c</sup> Values marked with an asterisk indicate measurements that may be biased by a spatially unresolved companion.

d Distances given with uncertainties are calculated from *Hipparcos* parallax measurements, while those without are kinematically estimated by Torres et al. (2008).

 $<sup>\</sup>overline{^5}$  The CHARA Array currently can reach K < 8.5 mag and V < 12 mag in excellent seeing conditions. These sensitivities are expected to become typical in average seeing conditions following the commissioning of adaptive optics systems on all six telescopes (ten Brummelaar et al. 2016).

here, HD 14082 A and B, make a 13."8 pair and V577 Per A has a companion at 9."5 that was not observed. HD 89744 has a massive planetary companion ( $m \sin i = 7.2 \, M_{\rm Jup}$ ) that orbits every 256 days in a highly eccentric orbit (e = 0.7; Korzennik et al. 2000), and an LOV proper motion companion at a separation of 63."0 (Wilson et al. 2001).

#### 2.2. Selection of Interferometric Calibrator Stars

A two-telescope optical/infrared interferometer measures the normalized power or visibility amplitude of the interference fringes (see Boden 2000 for a review). For a perfect system, an unresolved point source will have a normalized visibility of 1.0. The fringe amplitude for a spatially resolved source will be diminished below 1.0, because light across the stellar surface will combine incoherently. This reduction of the visibility amplitude depends on the angular size of the star. Loss of coherence can also be caused by instrumental and environmental effects.

To account for these instrumental effects and calibrate the system visibility, we observed single and effectively unresolved ( $\theta$  < 0.4 mas) stars before and after each science observation. These calibrator stars were selected using the getCal planning tool<sup>6</sup> distributed by the NASA Exoplanet Science Institute, which estimates the sizes of stars based on their photometric energy distributions. All selected calibrators lie within  $10^{\circ}$  on the sky and have  $K_s$  magnitudes within 1–2 magnitudes of their affiliated science star. To correct for the small but finite sizes of the calibrators, we adopted limbdarkened angular diameters for the calibrators provided by the SearchCal tool<sup>7</sup> developed by the JMMC Working Group (Bonneau et al. 2006, 2011). Diameters for three of our calibrators (HD 18682, HD 112943, and HD 154518) were not included in SearchCal. For these three stars, we used the V-Kcolor relation in Bonneau et al. (2006) to compute angular diameters based on the V magnitude from Kharchenko & Roeser (2009) and the 2MASS  $K_s$  magnitude (Skrutskie et al. 2006). Table 2 lists the HD numbers for all of the calibrators along with their spectral types assigned by Kharchenko & Roeser (2009), V and  $K_s$  magnitudes, adopted limb-darkened angular diameters, and the affiliated science star.

# 2.3. CHARA Array Observations and Data Reduction

The CHARA Array is an optical/infrared interferometer consisting of six 1 m telescopes arranged in a Y-configuration with baselines ranging from 34 to 331 m (ten Brummelaar et al. 2005). We observed the 13 young stars in our sample using the CHARA Classic beam combiner (ten Brummelaar et al. 2013). CHARA Classic combines the light from two telescopes simultaneously and scans through the fringe position using a dither mirror. Observations were obtained in both the *H*-band (1.6731  $\mu$ m center, 0.2854  $\mu$ m width) and *K'*-band (2.1329  $\mu$ m center, 0.3489  $\mu$ m width). To achieve the highest possible spatial resolution, we used the longest 331 m baseline between the S1 and E1 telescopes. A few of the observations for PX Vir were obtained with the 278 m baseline between the S1 and E2 telescopes, and some for HD 89744 were obtained with the 222 m baseline between the E1 and W2 telescopes. At the time when the measurements were collected, the detector readout mode for the H-band would saturate on bright targets.

**Table 2**Calibrator Properties

Calibrator	SpT	V	Ks	$\theta_{\rm LD}$ (mas)	Target
HD 691	K0V	7.939	6.176	$0.268 \pm 0.018$	HD 1405
HD 1083	A1V	6.342	6.328	$0.268 \pm 0.018$ $0.153 \pm 0.011$	HD 1405 HD 1405
HD 1003 HD 10126	G8V	7.730	6.040	$0.133 \pm 0.011$ $0.312 \pm 0.022$	HD 1403 HD 13482
HD 10120 HD 13382	G5V	7.730	5.786	$0.312 \pm 0.022$ $0.312 \pm 0.022$	HD 13482 HD 13482
HD 13382 HD 13836	G8V	8.123	6.448	$0.312 \pm 0.022$ $0.233 \pm 0.016$	HD 13482 HD 13482
HD 15836	F8V	7.486	6.170	$0.253 \pm 0.016$ $0.252 \pm 0.017$	HD 13482 HD 14082
HD 15320 HD 16397	G0V	7.360	5.833	$0.232 \pm 0.017$ $0.296 \pm 0.020$	HD 14082 HD 14082
HD 18682	K0V	7.780	5.170	$0.290 \pm 0.020$ $0.467 \pm 0.033$	HD 14082 HD 20385
HD 21038	A0V	6.501	6.340	$0.153 \pm 0.011$	HD 21845
HD 22879	F9V	6.684	5.179	$0.413 \pm 0.028$	HD 25457, HD
IID 22050	COM	7 472	5.006	0.201 + 0.010	20385
HD 23050	G2V	7.473	5.996	$0.281 \pm 0.019$	HD 21845
HD 23363	B7V	5.229	5.433	$0.206 \pm 0.014$	HD 25457
HD 25340	B5V	5.269	5.662	$0.165 \pm 0.011$	HD 25457
HD 54046	G0V	7.802	6.367	$0.234 \pm 0.016$	BD+20 1790
HD 55458	K1V	8.390	6.224	$0.272 \pm 0.019$	BD+20 1790
HD 57744	A1V	6.164	6.163	$0.161 \pm 0.011$	BD+20 1790
HD 87301	F4V	6.432	5.441	$0.334 \pm 0.023$	HIP 51317
HD 88725	G1V	7.738	6.153	$0.265 \pm 0.018$	HIP 51317
HD 90840	A4V	5.784	5.483	$0.206 \pm 0.014$	HD 89744
HD 91365	A2V	5.571	5.348	$0.274 \pm 0.019$	HD 89744
HD 91752	F3V	6.285	5.202	$0.382 \pm 0.026$	HD 89744
HD 111515	G8V	8.112	6.358	$0.246 \pm 0.017$	HD 113449
HD 112943	K7V	9.770	6.769	$0.232 \pm 0.016$	HD 113449
HD 117436	F2V	6.098	5.286	$0.346 \pm 0.024$	HD 113449
HD 153240	F6V	8.328	7.022	$0.169 \pm 0.012$	HD 152555
HD 154518	K2V	8.810	6.451	$0.254 \pm 0.018$	HD 152555
HD 157856	F3V	6.440	5.303	$0.365 \pm 0.025$	HD 152555
HD 202926	F6V	7.340	6.235	$0.235\pm0.016$	GJ 4199
HD 204079	K1V	8.295	6.202	$0.273 \pm 0.019$	GJ 4199
HD 206332	G0V	7.401	6.005	$0.276 \pm 0.019$	GJ 4199
HD 206374	G8V	7.443	5.774	$0.319 \pm 0.022$	GJ 4199

**Note.** The spectral types and V magnitudes are from Kharchenko & Roeser (2009); the  $K_s$  magnitudes are from 2MASS (Skrutskie et al. 2006); and the limb-darkened diameters are from SearchCal (Bonneau et al. 2006, 2011).

Aperture stops were used to attenuate the light when the counts were high enough to saturate the detector; this was needed for the *H*-band observations of GJ 159.

The recorded fringe data were reduced using the *reduceir* pipeline developed for CHARA Classic data (ten Brummelaar et al. 2005). The visibility amplitudes were computed by integrating the fringe power spectra. Log normal statistics were used to better represent the changes in correlation caused by atmospheric turbulence.

To calibrate the visibilities, we separated the calibrator and target observations into sequences observed under the same alignment conditions. Typically, we obtained several repeated observations on a given target, interspersed by calibrator observations. Using the adopted angular sizes of the calibrators (Table 2), we computed the expected visibilities of the calibrators assuming a uniform disk distribution of light. We then calculated the system visibility (the loss in fringe coherence due to the response of an imperfect interferometer) during each calibrator observation by comparing the measured and expected visibilities. We performed a linear least-squares fit to the set of calibrators in an observing sequence to determine the system visibility correction during the times of the target observations.

Table 3 lists the UT date and MJD of observation, the baseline used, the filter wavelength, the u and v coordinates of

<sup>6</sup> http://nexsci.caltech.edu/software/getCal/index.html

http://www.jmmc.fr/searchcal\_page.htm

 Table 3

 CHARA Classic Observations of Young Stars in AB Dor

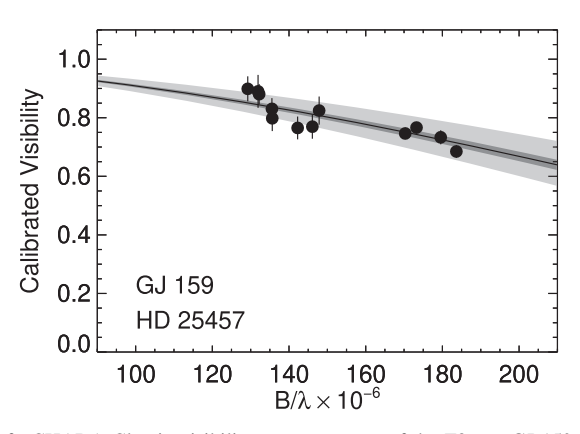
Object	UT Date	MJD	Baseline	λ	$u \times 10^{-6}$	$v \times 10^{-6}$	В	$V^{\mathbf{a}}$
				$(\mu m)$	(cycles/rad)	(cycles/rad)	(m)	
HD 25457	2008 Nov 17	54787.2619	S1-E1	2.1329	90.63	116.82	315.36	$0.825 \pm 0.048$
	2008 Nov 17	54787.2713	S1-E1	2.1329	87.76	116.80	311.60	$0.770 \pm 0.041$
	2008 Nov 17	54787.2896	S1-E1	2.1329	81.26	116.75	303.40	$0.765 \pm 0.039$
	2008 Nov 17	54787.3182	S1-E1	2.1329	68.97	116.69	289.11	$0.830 \pm 0.037$
	2008 Nov 17	54787.3321	S1-E1	2.1329	62.21	116.66	281.99	$0.881 \pm 0.034$
	2008 Nov 17	54787.3446	S1-E1	2.1329	55.67	116.64	275.66	$0.899 \pm 0.043$
	2008 Nov 18	54788.3152	S1-E1	2.1329	69.13	116.69	289.28	$0.798 \pm 0.044$
	2008 Nov 18	54788.3305	S1-E1	2.1329	61.61	116.66	281.39	$0.890 \pm 0.056$
	2009 Nov 16	55151.2846	S1-E1	1.6731	107.54	148.86	307.25	$0.685 \pm 0.021$
	2009 Nov 16	55151.2992	S1-E1	1.6731	100.48	148.82	300.42	$0.733 \pm 0.024$
	2009 Nov 16	55151.3202	S1-E1	1.6731	88.80	148.76	289.86	$0.766 \pm 0.017$
	2009 Nov 16	55151.3297	S1-E1	1.6731	82.96	148.73	284.94	$0.746 \pm 0.017$
HD 89744	2007 Nov 14	54418.4972	S1-E1	2.1329	98.94	103.43	305.30	$0.772 \pm 0.028$
	2007 Nov 14	54418.5051	S1-E1	2.1329	97.66	106.66	308.44	$0.799 \pm 0.031$
	2007 Nov 14	54418.5138	S1-E1	2.1329	95.96	110.15	311.60	$0.816 \pm 0.032$
	2007 Nov 14	54418.5218	S1-E1	2.1329	94.14	113.33	314.23	$0.781 \pm 0.034$
	2007 Nov 14	54418.5326	S1-E1	2.1329	91.31	117.48	317.37	$0.852 \pm 0.033$
	2008 May 12	54598.2014	E2-W1	2.1329	-95.05	-60.52	240.35	$0.882 \pm 0.251$
	2008 May 12	54598.2233	E2-W1	2.1329	-85.12	-68.71	233.33	$0.844 \pm 0.047$
	2008 May 12	54598.2316	E2-W1	2.1329	-80.91	-71.58	230.41	$0.990 \pm 0.391$
	2008 May 12	54598.2515	E2-W1	2.1329	-69.91	-77.83	223.15	$0.962 \pm 0.197$
	2008 May 12	54598.2604	E2-W1	2.1329	-64.67	-80.31	219.92	$0.903 \pm 0.095$
	2008 May 12	54598.2744	E2-W1	2.1329	-55.96	-83.83	214.97	$0.983 \pm 0.100$
	2008 May 12	54598.2838	E2-W1	2.1329	-49.88	-85.89	211.85	$0.916 \pm 0.155$
	2009 Apr 20	54941.3061	S1-E1	2.1329	-17.28	154.05	330.64	$0.834 \pm 0.092$
	2009 Apr 20	54941.3158	S1-E1	2.1329	-23.38	153.23	330.61	$0.808 \pm 0.052$
	2009 Apr 20	54941.3265	S1-E1	2.1329	-30.03	152.04	330.55	$0.857 \pm 0.026$
	2009 Apr 20	54941.3408	S1-E1	2.1329	-38.60	150.01	330.38	$0.832 \pm 0.081$
	2009 Apr 20	54941.3509	S1-E1	2.1329	-44.50	148.27	330.18	$0.832 \pm 0.059$
	2009 Apr 20	54941.3610	S1-E1	2.1329	-50.22	146.28	329.88	$0.884 \pm 0.051$
HIP 51317	2009 Apr 27	54948.1631	S1-E1	2.1329	60.61	118.22	283.36	$0.830 \pm 0.068$
	2009 Apr 27	54948.1852	S1-E1	2.1329	48.71	118.33	272.94	$0.894 \pm 0.064$
	2009 Apr 27	54948.1939	S1-E1	2.1329	43.77	118.37	269.18	$0.782 \pm 0.056$
	2009 Apr 27	54948.2095	S1-E1	2.1329	34.51	118.43	263.10	$0.879 \pm 0.046$
	2009 Apr 27	54948.2194	S1-E1	2.1329	28.54	118.46	259.89	$0.875 \pm 0.037$
	2009 Apr 27	54948.2288	S1-E1	2.1329	22.67	118.48	257.29	$0.860 \pm 0.047$
	2009 Apr 27	54948.2408	S1-E1	2.1329	15.11	118.50	254.79	$0.911 \pm 0.058$
	2009 Apr 30	54951.1716	S1-E1	1.6731	65.93	150.82	275.40	$0.767 \pm 0.047$
	2009 Apr 30	54951.1894	S1-E1	1.6731	53.07	150.92	267.66	$0.833 \pm 0.049$
	2009 Apr 30	54951.2141	S1-E1	1.6731	34.06	151.02	259.02	$0.926 \pm 0.056$
	2009 Apr 30	54951.2348	S1-E1	1.6731	17.51	151.07	254.45	$0.935 \pm 0.050$
	2009 May 01	54952.1838	S1-E1	2.1329	43.27	118.38	268.82	$0.843 \pm 0.067$
	2009 May 01	54952.2022	S1-E1	2.1329	32.37	118.44	261.88	$0.896 \pm 0.077$
	2009 Nov 15	55150.5005	S1-E1	2.1329	98.52	117.39	326.88	$0.819 \pm 0.044$
	2009 Nov 15	55150.5219	S1-E1	2.1329	94.27	117.58	321.44	$0.757 \pm 0.039$
	2009 Nov 15	55150.5402	S1-E1	2.1329	89.23	117.74	315.10	$0.811 \pm 0.044$
	2009 Nov 15	55150.5567	S1-E1	2.1329	83.71	117.87	308.36	$0.792 \pm 0.033$
	2009 Nov 16	55151.5156	S1-E1	1.6731	121.23	149.86	322.49	$0.720 \pm 0.056$
	2009 Nov 16	55151.5279	S1-E1	1.6731	117.31	149.99	318.59	$0.663 \pm 0.042$
	2009 Nov 16	55151.5418	S1-E1	1.6731	112.04	150.14	313.44	$0.710 \pm 0.044$
	2009 Nov 16	55151.5578	S1-E1	1.6731	104.93	150.30	306.69	$0.740 \pm 0.048$
	2009 Nov 16	55151.5643	S1-E1	1.6731	101.69	150.36	303.71	$0.809 \pm 0.041$
	2010 Apr 07	55293.2653	S1-E1	1.6731	43.63	150.98	262.93	$0.782 \pm 0.055$
	2010 Apr 07	55293.2821	S1-E1	1.6731	30.48	151.03	257.79	$0.765 \pm 0.050$
	2010 Apr 07 2010 Apr 07	55293.3002	S1-E1	1.6731	15.93	151.07	254.16	$0.766 \pm 0.058$
	2010 Apr 07 2010 Apr 07	55293.3196	S1-E1	1.6731	0.15	151.09	252.79	$0.759 \pm 0.047$
	2010 Apr 07 2010 Apr 07	55293.3306	S1-E1	1.6731	-8.86	151.08	253.21	$0.762 \pm 0.059$
	2010 Apr 07	33473.3300	91-E1	1.0/31	-0.00	131.00	433.41	0.702 ± 0.039

# Notes.

(This table is available in its entirety in machine-readable form.)

<sup>&</sup>lt;sup>a</sup> The visibility uncertainties for the three resolved stars have been scaled to force  $\chi^2_{\nu}=1$  for the best-fit limb-darkened model. The visibilities for the unresolved stars and the PX Vir binary are available online (the uncertainties for the unresolved targets have not been scaled).

<sup>&</sup>lt;sup>b</sup> The visibilities for HD 13482 have been corrected for the presence of incoherent light from the binary companion (see Section 2.4).



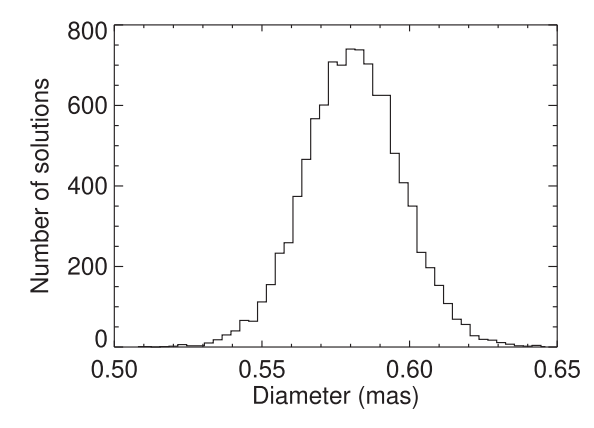


Figure 1. Left: CHARA Classic visibility measurements of the F8 star GJ 159 a proposed member of the AB Dor moving group. The visibility uncertainties were scaled to force the reduced  $\chi^2_{\nu}=1$  for the best-fit angular diameter. The black line shows the best-fit limb-darkened model, corresponding to an angular size of  $0.582\pm0.016$  mas. The shaded light gray region shows the range of angular diameters obtained from the bootstrap distribution, while the narrower dark gray region shows the standard deviation. A histogram of the bootstrap distribution is shown in the panel on the right.

the spatial frequencies projected on the sky in R.A. and decl., the length of the projected baseline B, and the calibrated visibility (V) for each star in our survey. The projected baseline is related to the spatial frequencies by  $B/\lambda = \sqrt{u^2 + v^2}$ . We discuss special reduction steps performed on HD 13482 and PX Vir in the next section.

# 2.4. Additional Reduction Notes for Individual Objects

HD 13482 has a companion at a separation of 1"8 and a magnitude difference of  $\Delta V = 1.6$  mag (Mason et al. 2001). The companion lies within the astronomical "seeing disk" (the Airy disk of the telescope convolved with the atmospheric seeing) of the primary star. As a consequence, the visibility measurements for this star are diminished because of incoherent light from its companion. Boyajian et al. (2008) provide a method for correcting for this effect, if the baseline length, detector pixel size, binary separation, flux ratio, and astronomical seeing are known (see their Equation (2)). During observations of HD 13482 the seeing, characterized by the Fried parameter  $r_0$  (Fried 1966), ranged from 4.0 to 7.8 cm. Using these values, along with the properties of the binary, the calibrated visibilities of HD 13482 were corrected for incoherent light from the companion. After applying the correction, the calibrated visibilities are consistent with a spatially unresolved primary star ( $V \sim 1.0$ ). These corrected visibilities are presented in Table 3.

The close companion in PX Vir also affects the measured visibilities. Using the available orbital data (Griffin 2010; Evans et al. 2012), we calculated that the binary had an expected projected separation of 20-40 mas along the baselines used during the CHARA observations. At these separations, we should be able to detect two fringe packets (one from each component) in the scan window (e.g., Farrington et al. 2010). However, given the brightness of the companion relative to the primary ( $\Delta H = 1.6$  mag) and the marginal seeing conditions, we were not able to detect reliably the fringe packet from the companion. During two out of a total of nine observations, we see evidence for a second fringe at ~30 mas projected separation, but the remaining scans from those nights are too noisy to confirm the detection. The visibilities measured for PX Vir in Table 3 are less than 1.0; this is likely attributed to incoherent light from the close companion diminishing the fringe amplitude of the primary star. Because of the difficulty in detecting the companion in these observations, we do not provide any further analysis for this target. Now that a preliminary visual orbit is known (Evans et al. 2012), appropriate baselines could be selected to optimize the detection of the companion and improve the orbital solution using additional observations with the CHARA Array.

#### 3. Results

Four of the 13 stars in our sample (GJ 159, GJ 393, HD 89744, and PX Vir) have calibrated visibilities significantly less than 1.0, consistent with being spatially resolved. We discuss the results for GJ 159, GJ 393, and HD 89744 in Section 3.1. As mentioned in Section 2.4, we were not able to obtain a reliable binary solution for PX Vir, although the companion is clearly affecting the measurements. The calibrated visibilities of the remaining nine stars are statistically indistinguishable from 1.0 and consistent with being spatially unresolved. These values are used to assign companion detection limits in Section 3.2.

# 3.1. The Angular Diameters of GJ 159, GJ 393, and HD 89744

The three resolved stars are GJ 159 (HD 25457), GJ 393 (HIP 51317), and HD 89744. The smoothly declining visibilities versus baseline length for all three stars (see Figures 1–3), observed consistently over many epochs, indicate that their photospheres are spatially resolved. For these, we computed both uniform disk ( $\theta_{\rm UD}$ ) and limb-darkened disk ( $\theta_{\rm LD}$ ) diameters by modeling the visibility data. The visibility of a uniform disk is described as

$$V = \frac{2J_1(x)}{r},\tag{1}$$

while the visibility of a limb-darkened disk is described as

$$V = \left[ (1 - \mu_{\lambda}) \frac{J_{1}(x)}{x} + \mu_{\lambda} \sqrt{\frac{\pi}{2}} \frac{J_{3/2}(x)}{x^{3/2}} \right] \times \left( \frac{1 - \mu_{\lambda}}{2} + \frac{\mu_{\lambda}}{3} \right)^{-1},$$
 (2)

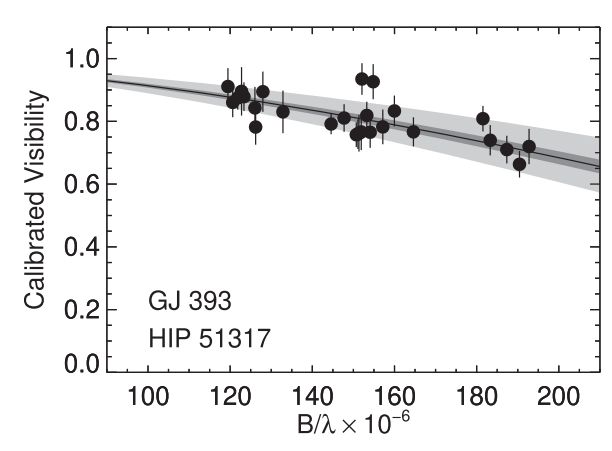


**Figure 2.** CHARA Classic visibility measurements of the M2.5 star GJ 393, a proposed member of the AB Dor moving group. The visibility uncertainties were scaled to force the reduced  $\chi^2_{\nu}=1$  for the best-fit angular diameter. The black line shows the best-fit limb-darkened model, corresponding to an angular size of  $0.564\pm0.021$  mas. The shaded light gray region shows the range of angular diameters obtained from the bootstrap distribution, while the narrower dark gray region shows the standard deviation.

where  $x = \pi B \theta \lambda^{-1}$ ,  $J_n$  is the *n*th order Bessel function, and  $\mu_{\lambda}$  is the wavelength-dependent limb-darkening coefficient (Hanbury Brown et al. 1974). Linear limb-darkening coefficients at H and K were adopted from Claret & Bloemen (2011) based on their computations using the least-square method and the ATLAS models. For GJ 159 and GJ 393, we adopted the effective temperatures 6200 K and 3420 K, respectively, assigned in the spectroscopic analysis of McCarthy & White (2012), and assumed log g values of 4.4 and 4.7 cm s<sup>-2</sup> based on the spectral types listed in Table 1 using the tabulation in Drilling & Landolt (2000). For HD 89744, we used an average effective temperature of 6222 K and  $\log g = 4.01 \text{ cm s}^{-2}$  based on the published values listed in Table 4 to determine the limbdarkening coefficients. The effective temperatures derived in Section 4 produce slightly different limb-darkening coefficients, but the effect on the angular diameters is negligible.

We computed the angular diameters by minimizing the  $\chi^2$ between the measured and model visibilities. For the limbdarkened model, the visibilities measured in the H- and K-bands were fit simultaneously. The uncertainties in the diameters were computed using a bootstrap technique (Efron & Tibshirani 1986; Press et al. 1992). From the observed distribution of visibility measurements, we randomly selected values with replacement to generate a new sample of visibilities consisting of the same total number of measurements. Because of the replacement, some measurements are repeated in the new sample and others are left out. We applied random Gaussian uncertainties to the new sample of visibilities based on the measurement errors. An angular diameter was fit to the new sample of visibilities and this process was repeated 10,000 times to generate the bootstrap distribution of angular diameters. The standard deviation of this distribution was adopted as the error on the angular diameter. During the bootstrap procedure, we scaled the uncertainty in the visibilities (the standard error output by the reduction pipeline) to force the reduced  $\chi^2_{\nu}$  to 1 for the best-fit limb-darkened model. This increased the visibility uncertainties by factors of 1.63, 2.41, and 1.12 for GJ 159, GJ 393, and HD 89744, respectively (the scaled visibility

**Table 4**Previously Published Stellar Properties

Star	$T_{\rm eff}$ (K)	[Fe/H]	$\log g \atop (\text{cm s}^{-2})$	References
GJ 159	6183			Muñoz Bermejo et al. (2013)
	6204			Muñoz Bermejo et al. (2013)
	6200			McCarthy & White (2012)
	6299	-0.06	4.36	Casagrande et al. (2011)
	6204	-0.03	4.30	Prugniel et al. (2007)
		+0.02	4.384	Lee et al. (2011)
		-0.014	4.388	Lee et al. (2011)
	6228	+0.04	4.29	Wu et al. (2011)
	6180	-0.10		Holmberg et al. (2009)
	6406			da Silva et al. (2009)
	6333		4.68	Schröder et al. (2009)
	6435	+0.18	4.68	Saffe and Gómez (2008)
	6515	-0.22	4.25	Saffe and Gómez (2008)
	6364	+0.00	4.68	Saffe and Gómez (2008)
	6219	+0.14		Ammons et al. (2006)
	6403	10.11		Masana et al. (2006)
	6333			Reiners (2006)
	6308		4.38	Gray et al. (2003)
	6190	-0.12	4.28	Prugniel & Soubiran (2001)
	6162	-0.12 $-0.11$		•
HD 89744		-0.11	4.28	Chen et al. (2000)
HD 89744	6270	+0.12	3.95	Bonfanti et al. (2016)
	6280	+0.13	3.97	Sitnova et al. (2015)
	6300	+0.24	4.07	Tsantaki et al. (2014)
	6242			Muñoz Bermejo et al. (2013)
	6222			Muñoz Bermejo et al. (2013)
	6349	+0.22	3.98	González Hernández
				et al. (2013)
	6095	+0.09	3.77	Mortier et al. (2013)
	6219	+0.23	3.95	Sansom et al. (2013)
	6262	+0.30	3.94	Casagrande et al. (2011)
		+0.267	4.149	Lee et al. (2011)
		+0.346	4.148	Lee et al. (2011)
	6169	+0.18	3.93	Prugniel et al. (2011)
	6196	+0.23	3.89	Schuler et al. (2011)
	6155	+0.15	3.95	Wu et al. (2011)
	6237	+0.17	3.88	Gonzalez et al. (2010)
	6223	+0.18		Holmberg et al. (2009)
	6236	+0.294	3.91	Chen et al. (2008)
	6281	+0.21	4.12	Prugniel et al. (2007)
	6186	+0.33	3.96	Schiavon (2007)
	0100	+0.256	2.50	Gonzalez & Laws (2007)
	6166	+0.04		Ammons et al. (2006)
	6149	10.04		Masana et al. (2006)
	6311	+0.22	4.37	Luck & Heiter (2006)
	6262	+0.22	3.98	Huang et al. (2005)
	6041	TU.29	3.70	Ramírez and Meléndez (2005)
		J N 14	3.91	Takeda et al. (2005)
	6188 6291	+0.14 +0.26	4.07	Valenti & Fischer (2005)
				` /
	6234	+0.22	3.98	Santos et al. (2004)
	6177	+0.18	3.89	Fuhrmann (2004)
	6202	. 0.22	3.99	Gray et al. (2003)
	6300	+0.22	4.40	Heiter & Luck (2003)
	6189		4.04	Ribas et al. (2003)
	6151	+0.13	4.04	Takeda et al. (2002)
	6338	+0.30	4.17	Gonzalez et al. (2001)
	6255	+0.18	4.00	Prugniel & Soubiran (2001)
	6186	+0.14	3.83	Gratton et al. (1996)
	6320	+0.18	4.07	Edvardsson et al. (1993)
	6083			Gray & Johanson (1991)
GJ 393	3544	-0.17	4.84	Maldonado et al. (2015)
	3548	-0.18		Mann et al. (2015)
	3511	-0.18		Newton et al. (2015)
		-0.19		Terrien et al. (2015)
	3514	-0.19		1 errien et al. (2015)

Table 4
(Continued)

Star	$T_{\rm eff}$ (K)	[Fe/H]	$\log g \atop (\text{cm s}^{-2})$	References
	3525	-0.18		Gaidos & Mann (2014)
	3500	-0.25	5.0	Malo et al. (2014)
	3431	-0.20		Neves et al. (2014)
		-0.18		Newton et al. (2014)
	3460		5.0	Lépine et al. (2013)
	3391	-0.22		Neves et al. (2013)
	3500		5.0	Rajpurohit et al. (2013)
	3500			Stelzer et al. (2013)
	3420			McCarthy & White (2012)
	3500			Zuckerman et al. (2011)
	5850			Bailer-Jones (2011)
	3570			da Silva et al. (2009)
	3403	-0.20		Casagrande et al. (2008)
	3524			Zickgraf et al. (2005)
	3325			Neff et al. (1995)
	3400			Giampapa et al. (1981)

uncertainties are reported in Table 3). The final limb-darkened diameters are  $0.582 \pm 0.016$  mas for GJ 159 (2.7% precision),  $0.564 \pm 0.021$  for GJ 393 (3.7% precision), and  $0.556 \pm 0.032$  mas for HD 89744 (5.9% precision). The measured uniform disk diameters at H and K, the adopted limb-darkening coefficients, and measured limb-darkened diameters are summarized in Table 5.

Of the three resolved stars, HD 89744 was observed only in the K-band, whereas observations of GJ 159 and GJ 393 were obtained at both H and K. This was because HD 89744 was observed as part of a program on measuring the angular diameters of exoplanet host stars using a different observing strategy; we present the measurements here because of its inclusion in our initial list of nearby moving group members. The angular diameter of HD 89744 is smaller than the formal resolution limit in the K-band on the longest baseline  $(0.5\lambda/B \sim 0.66 \,\mathrm{mas})$ . This is also the case for GJ 159 and GJ 393; however, the additional observations in the H-band for these two stars provide a factor of 1.3 improvement in resolution (0.52 mas). Because of the small angular size and lower instrumental resolution, we suspect that the interferometric measurements of HD 89744 could be influenced more strongly by systematic uncertainties in the visibility calibration. For example, if we fit limb-darkened diameters to the K-band visibilities only for GJ 159 and GJ 393, we get diameters larger than the combined fits by a factor of 1.0% and 4.6%, respectively. In contrast, if we fit only the H-band data, the difference from the combined fits are smaller by only 0.2% and 2.3%, respectively. This indicates that the diameters are constrained more stringently by the higher resolution data and that caution should be applied when evaluating angular diameters below the resolution of the instrument.

# 3.2. Angular Diameter Upper Limits

Nine of the 13 stars observed (PW And, HD 13482, HD 14082A, HD 14082B, HD 20385, V577 Per A, BD+20 1790, HD 152555, and LO Peg) have visibility measurements that are statistically indistinguishable from 1.0, and thus they are consistent with being spatially unresolved stars. These measurements can, nevertheless, be translated into an upper

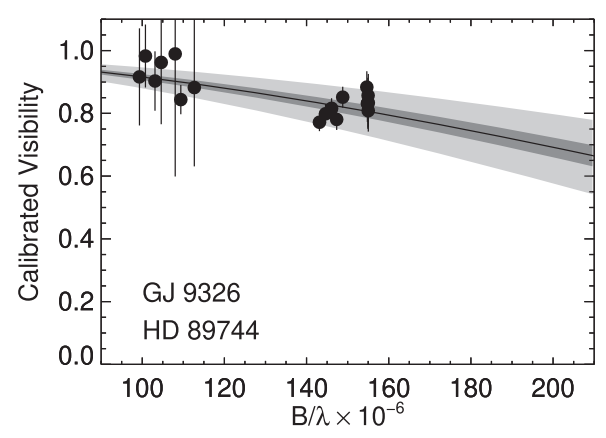


**Figure 3.** CHARA Classic visibility measurements of the F7 star HD 89744, a formerly proposed member of the AB Dor moving group. The visibility uncertainties were scaled to force the reduced  $\chi^2_{\nu}=1$  for the best-fit angular diameter. The black line shows the best-fit limb-darkened model, corresponding to an angular size of  $0.556\pm0.032$  mas. The shaded light gray region shows the range of angular diameters obtained from the bootstrap distribution, while the narrower dark gray region shows the standard deviation.

limit for the angular size of these stars. This can be done by estimating the typical uncertainty on the visibility measurements ( $\sigma_V$ ). We assume that the smallest star than can be resolved will have a visibility of  $V = 1-3\sigma_V$ . To estimate the effective resolution achieved during the observations, we convert this visibility into an angular diameter for a given baseline length and wavelength.

To accomplish this, we fit a uniform disk diameter to the visibility measurements for each star in our sample (excluding the binaries HD 13482 and PX Vir). We calculated the rms scatter about the uniform disk models as an assessment of the accuracy in any individual visibility measurement. This yielded an rms uncertainty in the visibilities of  $\sigma_V = 0.064$ , which translates to a  $3\sigma$  upper limit on the smallest angular size that can be measured of 0.43 mas. We also calculated the rms scatter about the limb-darkened disk models using only the two resolved sources (GJ 159, GJ 393) for which we collected the largest number of visibility measurements. This yielded an rms uncertainty in the visibilities of  $\sigma_V = 0.045$ , which translates to a  $3\sigma$  upper limit on the smallest angular size that can be reliably measured of 0.35 mas. This value is consistent with the smallest angular size measurement made with the CHARA Array at infrared (*H*-band) wavelengths (0.377  $\pm$  0.024 mas; Baines et al. 2007).

For the nine unresolved stars in our sample, the angular diameters estimated by McCarthy & White (2012) range from 0.19 to 0.32 mas. These sizes are smaller than the upper limit we computed of 0.35 mas. The combination of their physical radius and distance make their angular diameters too small to be resolved by our current observations.

# 3.3. Detection Limits on Small Separation (1–50 mas) Companions

Aside from the close binary PX Vir and the wide companion to HD 13482, the CHARA observations show no evidence that any of the remaining 11 stars have a close stellar companion. These results are consistent with previous non-detections in aperture masking and radial velocity surveys (e.g., Evans et al. 2012; Elliott et al. 2014).

Table 5
Angular Diameter Measurements

Star	Other	$\theta_{\mathrm{UDH}}$ (mas)	$\theta_{\mathrm{UDK}}$ (mas)	$\mu_H$	$\mu_{K}$	$\theta_{\mathrm{LD}}$ (mas)
GJ 159	HD 25457	$0.569 \pm 0.018$	$0.577 \pm 0.036$	0.274	0.240	$0.582 \pm 0.016$
GJ 393	HIP 51317	$0.542 \pm 0.029$	$0.582 \pm 0.022$	0.222	0.186	$0.564 \pm 0.021$
GJ 9326	HD 89744	•••	$0.546 \pm 0.032$	0.269	0.236	$0.556 \pm 0.032$

**Note.** The limb-darkening coefficients ( $\mu_H$  and  $\mu_K$ ) are from Claret & Bloemen (2011). The limb-darkened angular diameters for GJ 159 and GJ 393 are based on both H- and K-band interferometric measurements. For HD 89744, we obtained observations only in the K-band, which provides a lower instrumental resolution; given its small angular size, the diameter for HD 89744 could be more strongly influenced by systematic calibration uncertainties.

There are two ways that an interferometer can detect binary stars. If the separation is wide enough, then two separated fringe packets from each component will be observable in the scan window of the Classic beam combiner (e.g., Farrington et al. 2010). The minimum separation that will produce separated fringe packets is set by the coherence length of the filter  $(\lambda_0^2/\Delta\lambda)$ , which determines the overall shape and width of the fringe pattern. The maximum separation is set by the length of the dither scan (85  $\mu$ m for the short dither scan length used for most of the observations presented here). These limits correspond to a range of angular separation on the sky of 10-50 mas for the longest 331 m baseline for CHARA Classic operating in the near-infrared. We examined all data scans by eye, and did not find any separated fringe packet binaries in our sample. Based on the representative plots in Figure 2 of Farrington et al. (2010), we estimate that our visual inspection would have been sensitive to companions with magnitude differences brighter than  $\sim 1.0-1.5$  mag. This is consistent with the detection limits computed more formally by Raghavan et al. (2012). A companion in this field of view would also diminish the visibility of the primary fringe, due to incoherent light from the companion (see the discussion on HD 13482 in Section 2.4). Using the rms uncertainty of  $\sigma_V = 0.045$ (Section 3.2) provides a consistent estimate that we would have detected a depreciation of the visibility from a companion within this separation range with a magnitude difference brighter than 2.0 mag at the  $3\sigma$  level in average seeing conditions ( $r_0 \sim 6-8$  cm). The reduced visibilities that we measured for PX Vir are within these detection limits.

The other way to detect binaries with an interferometer is when the fringe packets of the two components overlap. In this case, the measured visibility will be modulated as a function of the projected baseline and binary separation on the sky (e.g., Boden 2000). The visibility curve versus baseline length becomes a periodic function where the separation between the peaks gives the projected separation of the binary and the visibility at the minimum is determined by the flux ratio  $f_2/f_1 = (1-V_{\min})/(1+V_{\min})$ . Using the rms uncertainty of  $\sigma_V = 0.045$ , we estimate that our observations would be sensitive to modulated fringe packet binaries down a flux ratio of 0.072 or magnitude difference of 2.9 mag at the  $3\sigma$  level. The range of separations for this detection limit would be set by the formal resolution limit of the interferometer  $\lambda/(2B) = 0.52$  mas for the longest 331 meter baseline in the H-band out to the  $\sim 10$  mas limit where binaries would be observed as separated fringe packets. However, we note that because the visibility curve of a close binary varies between  $V_{\min}$  and 1.0, that without sufficient time sampling with multiple baseline projections we cannot rule out absolutely a companion within these detection limits.

#### 4. Radii, Luminosities, and Temperatures

The stellar radii of GJ 159, GJ 393 and HD 89744 are determined from the measured limb-darkened angular diameters (Table 5) and distances provided by the *Hipparcos* parallaxes (van Leeuwen 2007; Table 1). These correspond to  $1.18 \pm 0.03~R_{\odot}$  (2.8% uncertainty) for GJ 159,  $0.43 \pm 0.02~R_{\odot}$  (4.0% uncertainty) for GJ 393, and  $2.36 \pm 0.14~R_{\odot}$  (5.9% uncertainty) for HD 89744; we define 1 solar radius to be 6.960 ×  $10^{10}$  cm, consistent with its mean measured value (Emilio et al. 2012).

We computed bolometric fluxes by fitting the observed SEDs. A summary of the magnitudes used for each star is presented in Table 6. We fit the SEDs using models and empirical spectral templates. As described below, we used different sets of models for the two F stars (GJ 159 and HD 89744) compared with the M-star (GJ 393). For each star, we converted the observed magnitudes  $m_{\lambda}$  to measured fluxes through

$$F_{\lambda,\text{meas}} = F_{\lambda_0} \times 10.0^{-0.4[m_{\lambda} - A_{\lambda}]},\tag{3}$$

where  $A_{\lambda}$  is the wavelength-dependent interstellar extinction assuming an R=3.1 reddening law (Cardelli et al. 1989; O'Donnell 1994), and  $F_{\lambda0}$  is the zero-point flux density for a filter at wavelength  $\lambda$  (e.g., Fukugita et al. 1995; Drilling & Landolt 2000). To compare the observed and model fluxes, we averaged the flux of the spectral models across the width of each filter band. The emergent flux from the star scales as the area subtended on the sky. Therefore, to find the best-fitting stellar model, we searched through a 3D grid in the scaling factor, interstellar extinction  $A_{V}$ , and effective temperature of the stellar model. We minimized the  $\chi^{2}$  between the observed and model fluxes to find the best-fit spectral model and determined uncertainties through a bootstrap method (e.g., the observed magnitudes are varied and the SED is re-fit, similar to the approach used for the visibility modeling in Section 3.1).

For GJ 159 and HD 89744, we fit the SEDs using low spectral resolution stellar models provided by R. Kurucz. Based on the published measurements of stellar properties tabulated in Table 4, the average metallicity for GJ 159 is [Fe/H] = -0.02, and that for HD 89744 is [Fe/H] = +0.21. The grid of models used for GJ 159 are therefore selected at solar metallicity ([Fe/H] = 0.00), while the grid used for HD 89744 are metal-rich ([Fe/H] = 0.20); the grids are available in  $\pm 0.20$  dex metallicity increments. Both grids assume  $\log g = 4.0$ , corresponding to a luminosity class intermediate to dwarfs and subgiants. The grids contain models calculated

<sup>8</sup> http://kurucz.harvard.edu/grids.html

**Table 6**Photometry Used in SED Fits

Star	Filter	Magnitude	References
GJ 159	Johnson U	$5.891 \pm 0.05$	Mermilliod et al. (1997)
GJ 159	Johnson B	$5.895 \pm 0.05$	Mermilliod et al. (1997)
GJ 159	Johnson $V$	$5.377\pm0.05$	Mermilliod et al. (1997)
GJ 159	Johnson B	$5.910 \pm 0.05$	Kharchenko &
			Roeser (2009)
GJ 159	Johnson $V$	$5.379 \pm 0.05$	Kharchenko &
			Roeser (2009)
GJ 159	Stromgren v	$6.155 \pm 0.08$	Hauck & Mermilliod (1998)
GJ 159	Stromgren b	$5.664 \pm 0.08$	Hauck & Mermilliod (1998)
GJ 159	Stromgren y	$5.342 \pm 0.08$	Hauck & Mermilliod (1998)
GJ 159	2MASS J	$4.712 \pm 0.236$	Skrutskie et al. (2006)
GJ 159	2MASS H	$4.342 \pm 0.076$	Skrutskie et al. (2006)
GJ 159	2MASS $K_s$	$4.181 \pm 0.036$	Skrutskie et al. (2006)
GJ 393	Johnson $U$	$12.349 \pm 0.05$	Koen et al. (2010)
GJ 393	Johnson B	$11.157 \pm 0.05$	Koen et al. (2010)
GJ 393	Johnson V	$9.631 \pm 0.05$	Koen et al. (2010)
GJ 393	Cousins $R_c$	$8.612 \pm 0.05$	Koen et al. (2010)
GJ 393	Cousins $I_c$	$7.393 \pm 0.05$	Koen et al. (2010)
GJ 393	Johnson $J$	$6.233 \pm 0.05$	Koen et al. (2010)
GJ 393	Johnson H	$5.582 \pm 0.05$	Koen et al. (2010)
GJ 393	Johnson K	$5.349 \pm 0.05$	Koen et al. (2010)
GJ 393	Johnson $U$	$12.389 \pm 0.05$	Landolt (2009)
GJ 393	Johnson B	$11.151 \pm 0.05$	Landolt (2009)
GJ 393	Johnson V	$9.650 \pm 0.05$	Landolt (2009)
GJ 393	Cousins $R_c$	$8.617 \pm 0.05$	Landolt (2009)
GJ 393	Cousins $I_c$	$7.389 \pm 0.05$	Landolt (2009)
GJ 393	Johnson B	$11.147 \pm 0.05$	Kharchenko &
			Roeser (2009)
GJ 393	Johnson V	$9.630 \pm 0.05$	Kharchenko &
			Roeser (2009)
GJ 393	2MASS J	$6.176 \pm 0.021$	Skrutskie et al. (2006)
GJ 393	2MASS H	$5.605 \pm 0.033$	Skrutskie et al. (2006)
GJ 393	2MASS $K_s$	$5.311 \pm 0.023$	Skrutskie et al. (2006)
HD 89744	Johnson $U$	$6.370 \pm 0.064$	Mermilliod et al. (1997)
HD 89744	Johnson B	$6.310 \pm 0.058$	Mermilliod et al. (1997)
HD 89744	Johnson V	$5.780 \pm 0.056$	Mermilliod et al. (1997)
HD 89744	Johnson B	$6.347 \pm 0.05$	Kharchenko &
			Roeser (2009)
HD 89744	Johnson V	$5.730 \pm 0.05$	Kharchenko &
			Roeser (2009)
HD 89744	Stromgren v	$6.579 \pm 0.08$	Hauck & Mermilliod (1998)
HD 89744	Stromgren b	$6.057 \pm 0.08$	Hauck & Mermilliod (1998)
HD 89744	Stromgren y	$5.719 \pm 0.08$	Hauck & Mermilliod (1998)
HD 89744	2MASS J	$4.855\pm0.232$	Skrutskie et al. (2006)
HD 89744	2MASS H	$4.529 \pm 0.036$	Skrutskie et al. (2006)
HD 89744	2MASS $K_s$	$4.454 \pm 0.021$	Skrutskie et al. (2006)

Note. Weighted mean UBV and uvby magnitudes were collected from the General Catalog of Photometric Data (http://obswww.unige.ch/gcpd/gcpd. html) maintained by Mermilliod et al. (1997), and from Hauck & Mermilliod (1998). The Stromgren indices b–y, m<sub>1</sub>, and c<sub>1</sub> were transformed to ubvy magnitudes using the transformations in Cousins & Caldwell (1985). and Turner (1990). We excluded the Stromgren u magnitude from the fit, because it was not consistent with the spectral models. We adopted minimum uncertainties of  $\pm 0.05$  for UBVRI and  $\pm 0.08$  for ubvy photometry. These uncertainties are assigned by the fbol routine in the getCal software and are based on an assessment of the typical variation of measured values (G. van Belle 2018, private communication).

with a temperature step size of 250 K. We interpolated between the templates to determine spectra at 50 K intervals.

For GJ 159, we found a best fit using the interpolated 6300 K spectral model with a visual extinction of  $0.01 \pm 0.13$  mag.

This temperature is consistent with the mean temperature of  $\sim$ 6292  $\pm$  107 K based on previously published measurements listed in Table 4. The low extinction is consistent with its close proximity (18.83  $\pm$  0.11 pc). Fixing  $A_V = 0.0$  and summing the flux of the best-fit model yields a bolometric flux of  $F_{\rm bol} = 1.762 \pm 0.097 \times 10^{-7} \, {\rm erg \, cm^{-2} \, s^{-1}}$ .

For HD 89744, we found a best fit using the interpolated 6150 K spectral model with a visual extinction of 0.01  $\pm$  0.15 mag. The effective temperature is slightly cooler than the mean value of 6222  $\pm$  72 K based on the previously published measurements listed in Table 4. The low extinction is consistent with the close proximity of the star (39.43  $\pm$  0.48 pc). Fixing  $A_V = 0.0$  and summing the flux of the best-fit model yields a bolometric flux of  $F_{\rm bol} = 1.272 \pm 0.061 \times 10^{-7} \, {\rm erg \, cm^{-2} \, s^{-1}}$ .

The SED and best-fitting spectral models for GJ 159 and HD 89744 are shown in Figure 4. The bolometric fluxes we computed for these two stars are lower by 4.5% and 4.8%, respectively ( $\sim 1\sigma$ ), compared with the values computed by Casagrande et al. (2011) using the infrared flux method ( $F_{\rm bol}=1.8407\times 10^{-7}~{\rm erg~cm^{-2}~s^{-1}}$  for HD 25457 and  $F_{\rm bol}=1.3326\times 10^{-7}~{\rm erg~cm^{-2}~s^{-1}}$  for HD 89744).

To check for systematic biases in our prescription, we also calculated the bolometric flux of GJ 159 and HD 89744 by fitting the SED using the stellar spectral flux library from Pickles (1998), which includes a range of stellar spectral type templates spanning wavelengths from 0.115 to 2.500  $\mu$ m. We used the Rayleigh-Jeans tail of a blackbody curve to approximate the flux at wavelengths longer than 2.5  $\mu$ m. For GJ 159, the best-fit stellar spectrum is that of an F5 dwarf, with a visual extinction of  $0.14 \pm 0.03$  mag. The non-zero extinction likely stems from the larger blueward flux of this slightly hotter best-fit template. However, we expect that this is likely unphysical given the close proximity of the star. If the visual extinction is set to zero, the best-fit spectrum is that of an F6 dwarf, with a bolometric flux of 1.793  $\pm$  0.082  $\times$  $10^{-7} \,\mathrm{erg}\,\mathrm{cm}^{-2}\,\mathrm{s}^{-1}$ . The computed  $F_{\mathrm{bol}}$  is consistent within the errors to the value computed using the Kurucz models. The spectral type is slightly hotter than the F8-like temperature inferred from the spectral analysis by (McCarthy & White 2012), but within the F5–F8 range of spectral types published earlier in the literature (Roman 1952; Malaroda 1975; Cowley 1976; Bidelman 1985; Gray 1989). For HD 89744, we find a best-fit stellar spectrum of an F8 dwarf, with a visual extinction of  $0.05^{+0.02}_{-0.05}$  mag. By fixing  $A_V = 0$  mag, we find a slightly cooler stellar spectrum of G0V and  $F_{\rm bol} = 1.289 \pm 0.098 \times 10^{-7} \, {\rm erg \, cm^{-2} \, s^{-1}}$ , consistent within the errors to  $F_{\rm bol}$  using the Kurucz models. Given this overall consistency, we choose to adopt the Kurucz values and uncertainties for GJ 159 and HD 89744.

The incomplete treatment of the TiO opacity in Kurucz atmospheric models (Castelli et al. 1997) make them less appropriate for determining the bolometric flux of the early M dwarf GJ 393. For this star, we fit the SED using flux-calibrated spectra from Mann et al. (2015). These templates provide improved spectral coverage and flux calibration for late-type stars compared with the Pickles stellar spectral flux library (Mann et al. 2013). GJ 393 (PM I10289+0050) itself is one of the stellar templates; Mann et al. (2015) derive a spectral type of M2.2, effective temperature of 3548 K, and metallicity of [Fe/H] = -0.18. This effective temperature is warmer than the value determined by McCarthy & White (2012; M2.5,

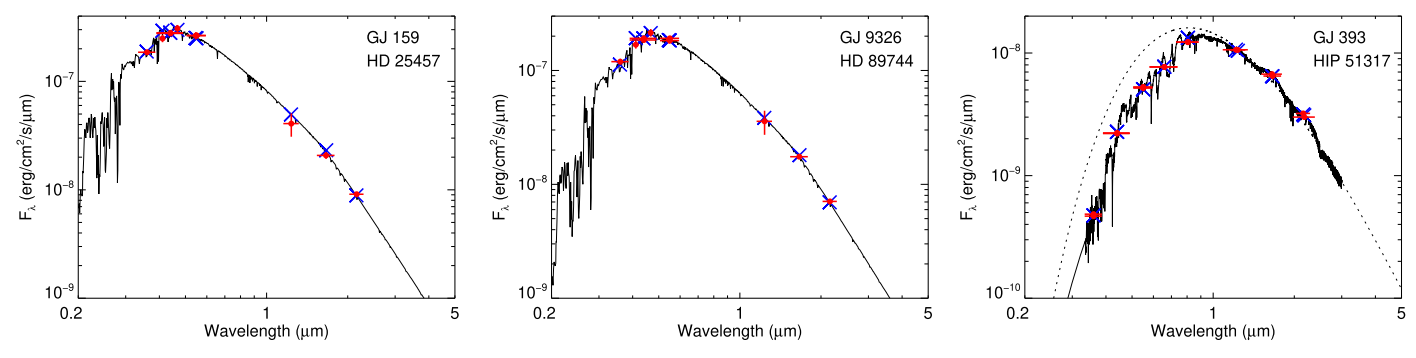


Figure 4. Spectral energy distributions for GJ 159 (left), HD 89744 (middle), and GJ 393 (right). For GJ 159 and HD 89744, we fit the photometric measurements using Kurucz spectral models. We found a best-fitting model with an effective temperature of 6300 K for GJ 159 and 6150 K for HD 89744, with an extinction consistent with  $A_V = 0$  mag. For GJ 393, we used the spectral templates from Mann et al. (2015) and found a best-fitting spectral type of M2.2 ( $T_{\rm eff} = 3548$  K) when fixing  $A_V = 0$ . For the Mann et al. templates, we used the Rayleigh–Jeans tail of a blackbody curve to approximate the flux at wavelengths longer than 3  $\mu$ m (dotted line). For GJ 393, this corresponds to about 10% of the total flux. The average flux of the stellar models across a given photometric band is shown by the blue crosses. The red symbols show the measured photometric magnitudes; the vertical length gives the size of the measurement error, while the horizontal width represents the width of the photometric filter.

 $T_{\rm eff}=3420~{\rm K})$  and the overall mean  $T_{\rm eff}=3476\pm66~{\rm K}$  based on the published values listed in Table 4. Fixing the visual extinction  $A_V=0.0$  mag, as expected based on the close proximity of the star (7.07  $\pm$  0.11 pc), and fitting the SED we recover GJ 393 as the best-fitting template and determine a bolometric flux of  $1.619\pm0.033\times10^{-8}~{\rm erg~cm^{-2}~s^{-1}}$  for GJ 393. This is consistent within  $0.2\sigma$  with the bolometric flux derived by Mann et al. (2015). The SED and best-fitting spectral template are shown in Figure 4.

For all three stars, we combined the bolometric fluxes with the Hipparcos distances to determine luminosities, which yield values of  $1.94\pm0.11~L_{\odot}$  for GJ 159 (5.7% uncertainty),  $0.0252\pm0.0009~L_{\odot}$  for GJ 393 (3.6% uncertainty), and  $6.15\pm0.33~L_{\odot}$  for HD 87944 (5.4% uncertainty). Finally, stellar effective temperatures are determined from the bolometric fluxes and limb-darkened angular diameters by inverting Stefan's Law,

$$F_{\text{bol}} = \frac{1}{4} \,\theta_{\text{LD}}^2 \sigma T_{\text{eff}}^4,\tag{4}$$

where  $\sigma$  is the Stefan–Boltzmann constant. This yields  $T_{\rm eff}=6286\pm123$  K for GJ 159 and  $T_{\rm eff}=3515\pm68$  K for GJ 393, consistent with previous  $T_{\rm eff}$  estimates. The uncertainties in these stellar effective temperature estimates are 1.9%; they are thus among the most precisely determined temperatures for adolescent-age single stars. The effective temperature for HD 89744 ( $T_{\rm eff}=5927\pm185$  K; 3.1%) is about 1.5 $\sigma$  lower than the average value of 6222  $\pm$  72 K based on spectroscopic and photometric measurements available in the literature (see Table 4). As discussed in Section 3.1, the lower instrumental resolution during the interferometric observations could have biased the diameter measurement of HD 89744. However, our SED fit also found a best-fitting template with a lower temperature of 6150 K. The stellar properties and results from the SED fits for each star are summarized in Table 7.

# 5. Mass and Age Estimates

5.1. GJ 159 and GJ 393

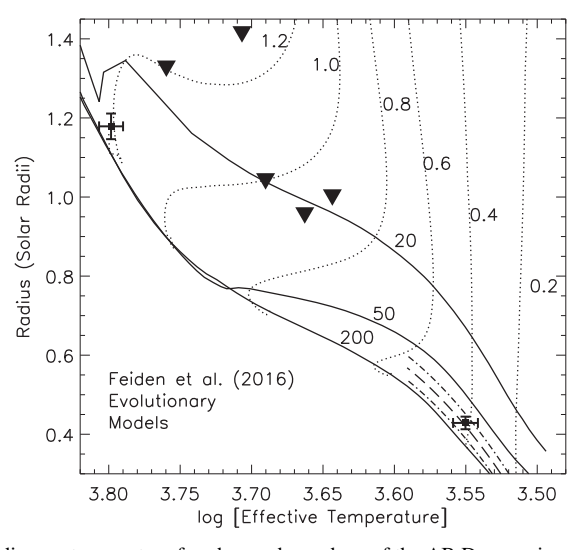
The measured radii and calculated temperatures for GJ 159 and GJ 393 are illustrated on a radius-temperature diagram in Figure 5. The stellar evolutionary models of Feiden (2016) and Baraffe et al. (2015), computed at solar metallicity, are shown

for comparison. We use these evolutionary models to create isochrones by linearly interpolating the mass tracks at specific ages; we note that this prescription yields isochrones consistent with nearby young associations (see Herczeg & Hillenbrand 2015) for both models. Solar metallicity is adopted as it is likely appropriate for members of the AB Dor moving group (Barenfeld et al. 2013) and GJ 159, but this is inconsistent with the measured subsolar metallicity of GJ 393. However, the changes in the model predictions using subsolar metallicity are less than the sizes of the error bars at the location of GJ 393. As Figure 5 illustrates, both stars lie within  $1.5\sigma$  of the zero-age main sequence (ZAMS), defined here as the loci of positions where low-mass stars have their smallest radii. Low-mass stars generally shrink in size as they approach the ZAMS, and then swell slowly thereafter. For approximate masses of 1.2  $M_{\odot}$  and  $0.45 M_{\odot}$  for GJ 159 and 393, the ZAMS occurs at ages of  $\sim 30$  Myr and  $\sim 200$  Myr, respectively.

Because evolutionary models have historically struggled to match the main sequence, especially at subsolar masses (e.g., Hillenbrand & White 2004; Torres et al. 2010; Bell et al. 2012; Feiden & Chaboyer 2012), we first test the predicted ZAMS near the position of GJ 393 through a comparison with an empirical main sequence determined from interferometric radius measurements of field K and M dwarfs<sup>9</sup> (Boyajian et al. 2013). As shown in Figure 5, this empirical main sequence is slightly cooler than the 200 Myr isochrone at 0.40  $M_{\odot}$  and the location of GJ 393. We note that this offset should not be a consequence of the assumed solar metallicity of the models; subsolar metallicity models will shift toward hotter temperatures and slightly smaller sizes, resulting in a larger offset from this empirical main sequence.

Aware of this possible discrepancy, both models predict that GJ 393 lies on the mass track of  $0.42 \pm 0.03~M_{\odot}$  at an age of  $80^{+40}_{-20}$  Myr if contracting toward the main sequence. The assigned uncertainties reflect only the uncertainties in the sizes and temperatures, and not those inherent to stellar evolutionary models. If GJ 393 is expanding away from the main sequence, then the lower limit on its age is set by the  $0.44~M_{\odot}$  track at 3 Gyr and the upper limit extends beyond the maximum age of

 $<sup>\</sup>overline{^9}$  The mean metallicity of the stars that define the empirical main sequence are slightly subsolar (mean [Fe/H] = -0.16 dex, with a standard deviation of +0.21 dex); it has a thickness of  $\pm 0.031$   $R_{\odot}$ .



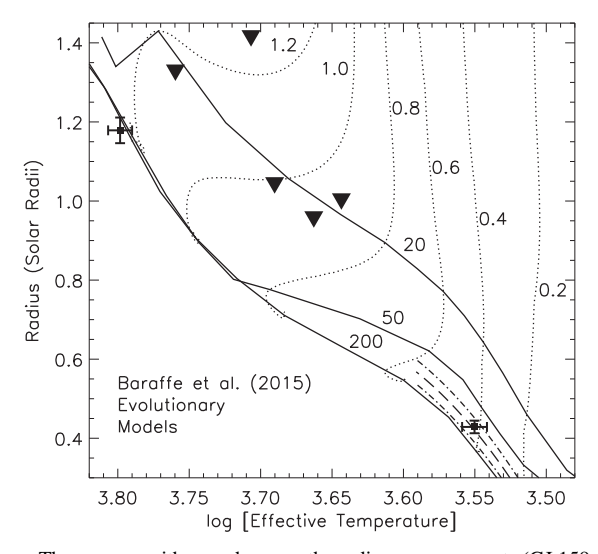


Figure 5. Radius vs. temperature for observed members of the AB Dor moving group. The squares with error bars are the radius measurements (GJ 159 and GJ 393) and the triangles are size upper limits. HD 152555 has a size upper limit of 1.8  $R_{\odot}$ , and is not shown in the graphs. For comparison, we plot mass tracks (dotted lines) and isochrones (solid lines), labeled in solar-mass units and millions of years, respectively, from the Feiden (2016) evolutionary models on the left and the Baraffe et al. (2015) models on the right. A portion of an empirical main sequence (dashed line), determined from interferometric measurements of field dwarfs, is also shown below  $0.6 M_{\odot}$ ; the dotted-dashed lines indicate the median absolute deviation of stars used to define this main sequence.

**Table 7**Stellar Properties

Quantity	GJ 159 HD 25457	GJ 393 HIP 51317	GJ 9326 HD 89744
Radius $(R_{\odot})$	$1.178 \pm 0.033$	$0.428 \pm 0.017$	$2.356 \pm 0.139$
Best-fit template	6300 K (Kurucz)	3548 K (Mann)	6150 K (Kurucz)
[Fe/H]	0.0 (fixed)	-0.18	0.2 (fixed)
$A_V$ (mag)	0.0 (fixed)	0.0 (fixed)	0.0 (fixed)
$F_{\text{bol}} (10^{-7} \text{ erg cm}^{-2} \text{ s}^{-1})$	$1.762 \pm 0.097$	$0.1619 \pm 0.0033$	$1.272 \pm 0.061$
$L\left(L_{\odot} ight)$	$1.944 \pm 0.110$	$0.0252 \pm 0.0009$	$6.153 \pm 0.332$
$T_{\rm eff}$ (K)	$6286 \pm 123$	$3515\pm68$	$5927 \pm 185$

Note. To determine the bolometric fluxes, we used synthetic Kurucz models for GJ 159 and HD 89744, and empirical spectral templates from Mann et al. (2015) for GJ 393. Because of its smaller angular size and the lower instrumental resolution during the interferometric observations of HD 89744 (see Section 3.1), the stellar properties of HD 89744 could be more strongly biased by systematic calibration uncertainties.

evolutionary models, calculated out to 20 Gyr by Feiden (2016) and 10 Gyr by Baraffe et al. (2015).

Testing the predicted ZAMS at 1.2  $M_{\odot}$  using size measurements of nearby F stars is inhibited by the larger spread in star sizes at this mass (Boyajian et al. 2012a) caused by their more rapid evolution. However, both evolutionary models show evidence of matching empirical main sequences defined by clusters and stars in the field at these masses (Baraffe et al. 2015; Feiden 2016). According to the Feiden (2016) models, GJ 159 lies on the mass track of  $1.21^{+0.09}_{-0.06}$   $M_{\odot}$  at an age of 23  $\pm$  2 Myr if contracting, or the mass track of 1.18 $^{+0.07}_{-0.05}$   $M_{\odot}$  at an age of  $2^{+1}_{-2}$  Gyr if expanding. We caution that ages and masses anywhere in between these most probable values are possible as the  $1\sigma$  error bars overlap the ZAMS. GJ 159 falls below, but within  $1\sigma$  of the Baraffe et al. ZAMS. According to these models the most probable mass for GJ 159 is only a few percent larger than that predicted by the Feiden (2016) models, and the age is restricted to be closer to the ZAMS.

The unresolved stars in the AB Dor moving group are plotted in Figure 5 using the upper limit on their angular diameters of 0.35 mas and their *Hipparcos* distances to compute an upper limit on their radii. We assigned

temperatures based on their spectral types in Table 1. Assuming that these stars also lie on the ZAMS, the measured size upper limits are between 40% and 90% larger than their actual radii (McCarthy & White 2012); longer baselines and/or observations at shorter wavelengths are needed to spatially resolve these stars.

# 5.2. HD 89744

As noted previously, HD 89744 is no longer considered a bona fide member of the AB Dor moving group. Although similar in temperature to GJ 159, HD 89744 is twice its size, confirming that it is a more evolved star. We note that slightly more massive stars cross this location while very young; this location is also consistent with that of a  $\sim$ 1.8  $M_{\odot}$  star at  $\sim$ 6 Myr, based on the pre-main sequence evolutionary calculations by Dotter et al. (2008) at a metallicity of [Fe/H] = +0.2 dex. The Dotter et al. (2008) evolutionary models, which are an older version of the Feiden (2016) models, are adopted in this case because they are publicly available at this metallicity; significant differences between these two generations of models are not expected in this mass range (G. Feiden 2018, private communication). This very

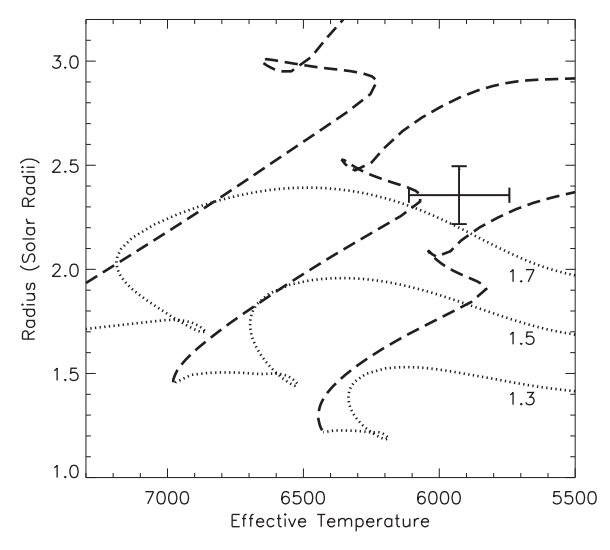


**Figure 6.** Radius vs. temperature for the formerly proposed AB Dor moving group member HD 89744. Super-solar metallicity ([Fe/H] =  $\pm$ 0.20 dex) mass tracks computed by Dotter et al. (2008) for 1.3, 1.5, and 1.7  $M_{\odot}$  are plotted as dotted lines up to an age of 100 Myr, then as dashed lines for older ages. Assuming HD 89744 is a post-main-sequence star, it has a mass of  $1.37 \pm 0.10 \ M_{\odot}$  and an age of  $3.8 \pm 0.9$  Gyr.

young age is considered unlikely given the slow rotation, absence of circumstellar material associated with HD 89744, and its depleted lithium abundance (Ramírez et al. 2012). Instead, as illustrated in Figure 6, the evolutionary models also yield a mass of  $1.37 \pm 0.10~M_{\odot}$  and age of  $3.8 \pm 0.9$  Gyr; the uncertainties span the range of possible values based on the  $1\sigma$  uncertainties in temperature and radius.

# 6. Summary and Discussion

We present interferometric measurements obtained with the CHARA Array of 12 adolescent-age stars in nearby moving groups, including one star in Tucana-Horologium, two stars in  $\beta$  Pictoris, and nine stars in AB Doradus. We also include measurements on HD 89744, which is no longer considered to be a member of the AB Dor moving group. We resolved the angular diameters of two members in the AB Dor subsample. Obtaining spatially resolved measurements of additional known members will require higher resolution (either by going to shorter wavelengths or using longer baselines), or a facility with equivalent resolution in the southern hemisphere.

The two spatially resolved candidate members of the AB Dor moving group are the F8 star GJ 159 (0.582  $\pm$  0.016 mas; 2.7% precision) and the M2.5 star GJ 393 (0.564  $\pm$  0.021 mas; 3.7% precision). We also resolved the previously suspected member HD 89744 (0.556  $\pm$  0.032 mas; 5.9% precision). We measured reduced visibilities for the known spectroscopic and visual binary PX Vir, but the available data are insufficient to reliably measure the separation during the observation. For the nine stars that were spatially unresolved, the measurements show no evidence for the presence of any close companions with separations in the range of 0.5–50 mas and near-infrared magnitude differences smaller than 2.0 magnitudes.

For GJ 159, GJ 393, and HD 89744, we used Stefan's Law to combine the angular diameters with bolometric fluxes derived from their photometric energy distributions to measure effective temperatures of  $6286 \pm 123 \, \text{K}$ ,  $3515 \pm 68 \, \text{K}$ , and  $5927 \pm 185 \, \text{K}$ , respectively. We compared the radius and temperature measurements to predictions from evolutionary

models to estimate masses and ages. Comparisons with the solar metallicity models computed by Feiden (2016) and Baraffe et al. (2015) yield masses of  $1.2 \pm 0.1~M_{\odot}$  for GJ 159 and  $0.42 \pm 0.03$  for GJ 393. Both stars are within  $1.5\sigma$  of the ZAMS, which inhibits assigning a precise age because it cannot be determined based on physical parameters alone whether the stars are contracting toward or expanding away from the ZAMS (e.g., Ligi et al. 2016). The age ranges derived for each star overlaps with the estimated age of the AB Dor moving group of 50–150 Myr (Malo et al. 2013; Bell et al. 2015).

For the F8 star GJ 159, model comparisons suggest a broad range of possible ages of 0.021-3.0 Gyr at the  $1\sigma$  uncertainty level. However, the detection of lithium in its atmosphere (e.g., Weise et al. 2010; McCarthy & White 2012) and a debris disk surrounding it (Hillenbrand et al. 2008) favor the interpretation that it lies near the ZAMS, with an age near the low end of this range (<100 Myr), consistent with its membership in the AB Dor moving group. Unfortunately the measurement and model uncertainties cannot exclude much older ages.

For GJ 393, the models suggest a broader range in age starting from 0.06 Gyr and extending beyond 10-20 Gyr at the  $1\sigma$  uncertainty level. As noted in Section 2.1, GJ 393 was a defining member of the AB Dor moving group (Torres et al. 2008; Malo et al. 2013); however, Bell et al. (2015) find that it is hotter and/or under-luminous relative to the single-star isochrone for the group. This is consistent with it being an older metal-poor star. In support of this, we note the lack of youthful characteristics. GJ 393 is slowly rotating (v sin  $i = 1.5 \text{ km s}^{-1}$ ; Reiners 2007) and chromospherically inactive relative to other proposed early M dwarf members (e.g., V372 Pup,  $v \sin i = 20 \text{ km s}^{-1}$ ; da Silva et al. 2009). Precision radial velocity measurements of GJ 393 have achieved values consistent to within a few m s<sup>-1</sup>, spanning several years time (Bonfils et al. 2013), which is uncharacteristic of young adolescent-age M dwarfs (e.g., Paulson & Yelda 2006). We conclude that GJ 393 is likely an old field star that coincidentally has a space motion similar to that of bonafide AB Dor members; it is probably a kinematic interloper.

The size and temperature of the planet host and wide binary star HD 89744 confirm that it has evolved off the main sequence. A comparison with evolutionary models with a metallicity of [Fe/H] = +0.15 dex computed by Dotter et al. (2008) yields a mass of  $1.37 \pm 0.10$   $M_{\odot}$  at an age of  $3.8 \pm 0.9$  Gyr. We caution that the assigned errors are approximate, as the evolution is nonlinear in both time and the radius-temperature plane at this evolutionary stage. Values assigned for stars near the "hook region" of the HR diagram are known to be ambiguous (Edvardsson et al. 1993). Nevertheless, the age is slightly larger, but statistically consistent with the range of previous age estimates (1.5-3.0 Gyr) assembled in Wilson et al. (2001). Additional interferometric measurements at higher angular resolution could help confirm the radius and effective temperature measured for HD 89744 and its estimated older age which could impact whether the LOV companion identified by Wilson et al. (2001) is a brown dwarf or a very low-mass star.

This work is based upon observations obtained with the Georgia State University Center for High Angular Resolution Astronomy Array at Mount Wilson Observatory. The CHARA Array is supported by the National Science Foundation under grant AST-1211929. Institutional support has been provided

from the GSU College of Arts and Sciences and the GSU Office of the Vice President for Research and Economic Development. We thank Mount Wilson Institute for providing infrastructure support at the Observatory. We thank P. J. Goldfinger for providing operational support at the CHARA Array, and Y. Touhami for collecting data during some of the observations. We thank A. Mann for providing the spectral templates for late-type stars, M. Simon for useful discussions on the evolutionary models at young stellar ages, and G. Herczeg for helpful comments that led to improvements in the manuscript. G. H. Schaefer acknowledges support from NSF grant AST-1411654. R. J. White acknowledges support from NSF grant AST-1517762. This research has made use of the SIMBAD database and VizieR catalog service operated at CDS in Strasbourg, France, the SearchCal tool developed by the Jean-Marie Mariotti Center, and the getCal software developed by the NASA Exoplanet Science Institute at the California Institute of Technology.

Facility: CHARA.

*Software:* reduceir (ten Brummelaar 2014), SearchCal (Bonneau et al. 2006, 2011), getCal (http://nexsci.caltech.edu/software/getCal/index.html).

#### **ORCID iDs**

```
R. J. White https://orcid.org/0000-0001-5313-7498
E. K. Baines https://orcid.org/0000-0002-5684-3424
T. S. Boyajian https://orcid.org/0000-0001-9879-9313
T. A. ten Brummelaar https://orcid.org/0000-0002-0114-7915
C. D. Farrington https://orcid.org/0000-0001-9939-2830
```

G. H. Schaefer https://orcid.org/0000-0001-5415-9189

#### References

```
Aller, K. M., Liu, M. C., Magnier, E. A., et al. 2016, ApJ, 821, 120
Ammons, S. M., Robinson, S. E., Strader, J., et al. 2006, ApJ, 638, 1004
Bailer-Jones, C. A. L. 2011, MNRAS, 411, 435
Baines, E. K., van Belle, G. T., ten Brummelaar, T. A., et al. 2007, ApJL,
   661, L195
Baraffe, I., Homeier, D., Allard, F., & Chabrier, G. 2015, A&A, 577, A42
Barenfeld, S. A., Bubar, E. J., Mamajek, E. E., & Young, P. A. 2013, ApJ,
  766, 6
Bell, C. P. M., Mamajek, E. E., & Naylor, T. 2015, MNRAS, 454, 593
Bell, C. P. M., Naylor, T., Mayne, N. J., Jeffries, R. D., & Littlefair, S. P. 2012,
   MNRAS, 424, 3178
Bessell, M. S. 2000, PASP, 112, 961
Bidelman, W. P. 1985, ApJS, 59, 197
Boden, A. F. 2000, in Principles of Long Baseline Stellar Interferometry, ed.
  P. R. Lawson (Pasadena, CA: JPL), 9
Boden, A. F., Torres, G., Sargent, A. I., et al. 2007, ApJ, 670, 1214
Bonfanti, A., Ortolani, S., & Nascimbeni, V. 2016, A&A, 585, A5
Bonfils, X., Delfosse, X., Udry, S., et al. 2013, A&A, 549, A109
Bonneau, D., Clausse, J.-M., Delfosse, X., et al. 2006, A&A, 456, 789
Bonneau, D., Delfosse, X., Mourard, D., et al. 2011, A&A, 535, A53
Boyajian, T. S., McAlister, H. A., Baines, E. K., et al. 2008, ApJ, 683, 424
Boyajian, T. S., McAlister, H. A., van Belle, G., et al. 2012a, ApJ, 746, 101
Boyajian, T. S., von Braun, K., van Belle, G., et al. 2012b, ApJ, 757, 112
Boyajian, T. S., von Braun, K., van Belle, G., et al. 2013, ApJ, 771, 40
Cardelli, J. A., Clayton, G. C., & Mathis, J. S. 1989, ApJ, 345, 245
Casagrande, L., Flynn, C., & Bessell, M. 2008, MNRAS, 389, 585
Casagrande, L., Schönrich, R., Asplund, M., et al. 2011, A&A, 530, A138
Castelli, F., Gratton, R. G., & Kurucz, R. L. 1997, A&A, 318, 841
Chauvin, G., Lagrange, A.-M., Dumas, C., et al. 2004, A&A, 425, L29
Chen, Y. Q., Nissen, P. E., Zhao, G., Zhang, H. W., & Benoni, T. 2000,
      AS. 141, 491
Chen, Y. Q., Zhao, G., Izumiura, H., et al. 2008, AJ, 135, 618
Claret, A., & Bloemen, S. 2011, A&A, 529, A75
Cousins, A. W. J., & Caldwell, J. A. R. 1985, Obs, 105, 134
```

```
Cowley, A. P. 1976, PASP, 88, 95
da Silva, L., Torres, C. A. O., de La Reza, R., et al. 2009, A&A, 508, 833
Dotter, A., Chaboyer, B., Jevremović, D., et al. 2008, ApJS, 178, 89
Drilling, J. S., & Landolt, A. U. 2000, in Allens Astrophysical Quantities, ed.
   A. N. Cox (New York: AIP), 381
Edvardsson, B., Andersen, J., Gustafsson, B., et al. 1993, A&A, 275, 101
Efron, B., & Tibshirani, R. 1986, StaSc, 1, 54
Elliott, P., Bayo, A., Melo, C. H. F., et al. 2014, A&A, 568, A26
Emilio, M., Kuhn, J. R., Bush, R. I., & Scholl, I. F. 2012, ApJ, 750, 135
Evans, T. M., Ireland, M. J., Kraus, A. L., et al. 2012, ApJ, 744, 120
Farrington, C. D., ten Brummelaar, T. A., Mason, B. D., et al. 2010, AJ,
  139, 2308
Feiden, G. A. 2016, A&A, 593, A99
Feiden, G. A., & Chaboyer, B. 2012, ApJ, 757, 42
Fried, D. L. 1966, JOSA, 56, 1372
Fuhrmann, K. 2004, AN, 325, 3
Fukugita, M., Shimasaku, K., & Ichikawa, T. 1995, PASP, 107, 945
Gaidos, E., & Mann, A. W. 2014, ApJ, 791, 54
Giampapa, M. S., Worden, S. P., Schneeberger, T. J., & Cram, L. E. 1981, ApJ,
Gonzalez, G., Carlson, M. K., & Tobin, R. W. 2010, MNRAS, 403, 1368
Gonzalez, G., & Laws, C. 2007, MNRAS, 378, 1141
Gonzalez, G., Laws, C., Tyagi, S., & Reddy, B. E. 2001, AJ, 121, 432
González Hernández, J. I., Delgado-Mena, E., Sousa, S. G., et al. 2013, A&A,
Gratton, R. G., Carretta, E., & Castelli, F. 1996, A&A, 314, 191
Gray, D. F., & Johanson, H. L. 1991, PASP, 103, 439
Gray, R. O. 1989, AJ, 98, 1049
Gray, R. O., Corbally, C. J., Garrison, R. F., McFadden, M. T., &
   Robinson, P. E. 2003, AJ, 126, 2048
Griffin, R. F. 2010, Obs, 130, 125
Guenther, E. W., & Tal-Or, L. 2010, A&A, 521, A83
Hanbury Brown, R., Davis, J., Lake, R. J. W., & Thompson, R. J. 1974,
         AS, 167, 475
Hauck, B., & Mermilliod, M. 1998, A&AS, 129, 431
Heiter, U., & Luck, R. E. 2003, AJ, 126, 2015
Herczeg, G. J., & Hillenbrand, L. A. 2015, ApJ, 808, 23
Hillenbrand, L. A., Carpenter, J. M., Kim, J. S., et al. 2008, ApJ, 677, 630
Hillenbrand, L. A., & White, R. J. 2004, ApJ, 604, 741
Høg, E., Fabricius, C., Makarov, V. V., et al. 2000, A&A, 355, L27
Holmberg, J., Nordström, B., & Andersen, J. 2009, A&A, 501, 941
Huang, C., Zhao, G., Zhang, H. W., & Chen, Y. Q. 2005, MNRAS, 363, 71
Kalas, P., Liu, M. C., & Matthews, B. C. 2004, Sci, 303, 1990
Kataria, T., & Simon, M. 2010, AJ, 140, 206
Kharchenko, N. V., & Roeser, S. 2009, yCat, 1280, 0
Koen, C., Kilkenny, D., van Wyk, F., & Marang, F. 2010, MNRAS, 403, 1949
Korzennik, S. G., Brown, T. M., Fischer, D. A., Nisenson, P., & Noyes, R. W.
   2000, ApJL, 533, L147
Landolt, A. U. 2009, AJ, 137, 4186
Le Bouquin, J.-B., Monin, J.-L., Berger, J.-P., et al. 2014, A&A, 561, A101
Lee, Y. S., Beers, T. C., Allende Prieto, C., et al. 2011, AJ, 141, 90
Lépine, S., Hilton, E. J., Mann, A. W., et al. 2013, AJ, 145, 102
Ligi, R., Creevey, O., Mourard, D., et al. 2016, A&A, 586, A94
Liu, M. C. 2004, Sci, 305, 1442
López-Santiago, J., Montes, D., Crespo-Chacón, I., & Fernández-Figueroa, M. J.
   2006, ApJ, 643, 1160
Luck, R. E., & Heiter, U. 2006, AJ, 131, 3069
Luhman, K. L., Stauffer, J. R., Muench, A. A., et al. 2003, ApJ, 593, 1093
Malaroda, S. 1975, AJ, 80, 637
Maldonado, J., Affer, L., Micela, G., et al. 2015, A&A, 577, A132
Malo, L., Doyon, R., Feiden, G. A., et al. 2014, ApJ, 792, 37
Malo, L., Doyon, R., Lafrenière, D., et al. 2013, ApJ, 762, 88
Mamajek, E. E., & Bell, C. P. M. 2014, MNRAS, 445, 2169
Mann, A. W., Feiden, G. A., Gaidos, E., Boyajian, T., & von Braun, K. 2015,
Mann, A. W., Gaidos, E., & Ansdell, M. 2013, ApJ, 779, 188
Masana, E., Jordi, C., & Ribas, I. 2006, A&A, 450, 735
Mason, B. D., Hartkopf, W. I., Wycoff, G. L., & Wieder, G. 2007, AJ,
Mason, B. D., Wycoff, G. L., Hartkopf, W. I., Douglass, G. G., &
   Worley, C. E. 2001, AJ, 122, 3466
McCarthy, K., & White, R. J. 2012, AJ, 143, 134
Mermilliod, J.-C., Mermilliod, M., & Hauck, B. 1997, A&AS, 124, 349
Mortier, A., Santos, N. C., Sousa, S. G., et al. 2013, A&A, 557, A70
Muñoz Bermejo, J. M., Asensio Ramos, A., & Allende Prieto, C. 2013, A&A,
   553, 95
```

```
Neff, J. E., O'Neal, D., & Saar, S. H. 1995, ApJ, 452, 879
Neves, V., Bonfils, X., Santos, N. C., et al. 2013, A&A, 551, A36
Neves, V., Bonfils, X., Santos, N. C., et al. 2014, A&A, 568, A121
Newton, E. R., Charbonneau, D., Irwin, J., et al. 2014, AJ, 147, 20
Newton, E. R., Charbonneau, D., Irwin, J., & Mann, A. W. 2015, ApJ, 800, 85
Nomura, H., Tsukagoshi, T., Kawabe, R., et al. 2016, ApJL, 819, L7
O'Donnell, J. E. 1994, ApJ, 422, 158
Paulson, D. B., & Yelda, S. 2006, PASP, 118, 706
Pecaut, M. J., & Mamajek, E. E. 2013, ApJS, 208, 9
Pickles, A. J. 1998, PASP, 110, 863
Press, W. H., Teukolsky, S. A., Vetterling, W. T., & Flannery, B. P. 1992,
  Numerical Recipes in C: The Art of Scientific Computing (New York:
   Cambridge Univ. Press)
Prugniel, P., & Soubiran, C. 2001, A&A, 369, 1048
Prugniel, P., Soubiran, C., Koleva, M., & Le Borgne, D. 2007, arXiv:astro-ph/
   0703658
Prugniel, P., Vauglin, I., & Koleva, M. 2011, A&A, 531, A165
Raghavan, D., Farrington, C. D., ten Brummelaar, T. A., et al. 2012, ApJ,
Rajpurohit, A. S., Reylé, C., Allard, F., et al. 2013, A&A, 556, A15
Ramírez, I., Fish, J. R., Lambert, D. L., & Allende Prieto, C. 2012, ApJ, 756, 46
Ramírez, I., & Meléndez, J. 2005, ApJ, 626, 446
Reiners, A. 2006, A&A, 446, 267
Reiners, A. 2007, A&A, 467, 259
Ribas, I., Solano, E., Masana, E., & Giménez, A. 2003, A&A, 411, L501
Riedel, A. R., Blunt, S. C., Lambrides, E. L., et al. 2017, AJ, 153, 95
Roman, N. G. 1952, ApJ, 116, 122
Saffe, C., Gómez, M., Pintado, O., & González, E. 2008, A&A, 490, 297
Sansom, A. E., de Castro Milone, A., Vazdekis, A., & Sánchez-Blázquez, P.
  2013, MNRAS, 435, 952
Santos, N. C., Israelian, G., & Mayor, M. 2004, A&A, 415, 1153
Schiavon, R. P. 2007, ApJS, 171, 146
Schlieder, J. E., Lépine, S., & Simon, M. 2010, AJ, 140, 119
Schneider, A. C., Windsor, J., Cushing, M. C., Kirkpatrick, J. D., &
   Wright, E. L. 2016, ApJL, 822, L1
Schröder, C., Reiners, A., & Schmitt, J. H. M. M. 2009, A&A, 493, 1099
Schuler, S. C., Flateau, D., Cunha, K., et al. 2011, ApJ, 732, 55
```

```
Sitnova, T., Zhao, G., Mashonkina, L., et al. 2015, ApJ, 808, 148
Skrutskie, M. F., Cutri, R. M., Stiening, R., et al. 2006, AJ, 131, 1163
Stauffer, J. R., Hartmann, L. W., Fazio, G. G., et al. 2007, ApJS, 172, 663
Stelzer, B., Marino, A., Micela, G., López-Santiago, J., & Liefke, C. 2013,
   MNRAS, 431, 2063
Takeda, Y., Ohkubo, M., Sato, B., Kambe, E., & Sadakane, K. 2005, PASJ,
  57, 27
Takeda, Y., Sato, B., Kambe, E., Sadakane, K., & Ohkubo, M. 2002, PASJ,
  54, 1041
ten Brummelaar, T. 2014, in EAS Publications Ser. 69, What the Highest Angular
  Resolution Can Bring to Stellar Astrophysics?, ed. F. Millour et al. (Les Ulis:
  EDP Sciences), 101
ten Brummelaar, T. A., Gies, D. G., McAlister, H. A., et al. 2016, Proc. SPIE,
  9907, 990703
ten Brummelaar, T. A., McAlister, H. A., Ridgway, S. T., et al. 2005, ApJ,
  628, 453
ten Brummelaar, T. A., Sturmann, J., Ridgway, S. T., et al. 2013, JAI, 2, 40004
Terrien, R. C., Mahadevan, S., Deshpande, R., & Bender, C. F. 2015, ApJS,
Torres, C. A. O., Quast, G. R., Melo, C. H. F., & Sterzik, M. F. 2008, in
  Handbook of Star Forming Regions, Vol. II, ed. B. Reipurth (California:
  ASP Monographs), 757
Torres, G., Andersen, J., & Giménez, A. 2010, A&ARv, 18, 67
Tsantaki, M., Sousa, S. G., Santos, N. C., et al. 2014, A&A, 570, A80
Turner, D. G. 1990, PASP, 102, 1331
Valenti, J. A., & Fischer, D. A. 2005, ApJS, 159, 141
van Leeuwen, F. 2007, A&A, 474, 653
Weise, P., Launhardt, R., Setiawan, J., & Henning, T. 2010, A&A, 517,
  A88
White, R. J., Ghez, A. M., Reid, I. N., & Schultz, G. 1999, ApJ, 520, 811
Wilson, J. C., Kirkpatrick, J. D., Gizis, J. E., et al. 2001, AJ, 122, 1989
Wu, Y., Singh, H. P., Prugniel, P., Gupta, R., & Koleva, M. 2011, A&A,
Zickgraf, F.-J., Krautter, J., Reffert, S., et al. 2005, A&A, 433, 151
Zuckerman, B., Rhee, J. H., Song, I., & Bessell, M. S. 2011, ApJ, 732, 61
Zuckerman, B., & Song, I. 2004, ARA&A, 42, 685
```

Simon, M., & Schaefer, G. H. 2011, ApJ, 743, 158